A Homonuclear Molecule with a Permanent Electric Dipole Moment

W. Li, *et al.*

Science **334**, 1110 (2011);
DOI: 10.1126/science.1211255

Energy in the United States; Commissariat à l'Energie Atomique et aux Énergies Alternatives, Institut de Recherche sur les Lois Fondamentales de l'Univers (CEA/IRFU) and Institut National de Physique Nucléaire et de Physique des Particules, Centre National de la Recherche Scientifique (IN2P3/CNRS) in France; Agenzia Spaziale Italiana (ASI) and Istituto Nazionale di Fisica Nucleare (INFN) in Italy; Ministry of Education, Culture, Sports, Science, and Technology (MEXT), Energy Accelerator Research Organization (KEK), and Japan Aerospace Exploration Agency (JAXA) in Japan; and the K. A. Wallenberg Foundation, Swedish Research Council, and National Space Board in Sweden. Additional support from Istituto Nazionale di Astrofisica (INAF) in Italy and Centre National d'Etudes Spaciales (CNES) in France for science analysis during the operations phase is also gratefully acknowledged. The Nançay Radio Observatory is operated by the Paris Observatory, associated with the French CNRS. The Lovell Telescope is owned and operated by the University of Manchester as part of the Jodrell Bank Centre for Astrophysics with support from the Science and Technology Facilities Council of the United Kingdom. Fermi LAT data, γ-ray diffuse models, and radio pulsar ephemeris are available from the Fermi Science Support Center (http://fermi.gsfc.nasa.gov/ssc/data/access). M.L.-G. was funded by contract ERC-StG-259391 from the European Community. E.T. is a NASA Postdoctoral Program Fellow. We thank the anonymous referees for their very constructive suggestions.

The Fermi LAT Collaboration

P. C. C. Freire,[1]† A. A. Abdo,[2]‡ M. Ajello,[3] A. Allafort,[3] J. Ballet,[4] G. Barbiellini,[5,6] D. Bastieri,[7,8] K. Bechtol,[3] R. Bellazzini,[9] R. D. Blandford,[3] E. D. Bloom,[3] E. Bonamente,[10,11] A. W. Borgland,[3] M. Brigida,[12,13] P. Bruel,[14] R. Buehler,[3] S. Buson,[7,8] G. A. Caliandro,[15] R. A. Cameron,[3] F. Camilo,[16] P. A. Caraveo,[17] C. Cecchi,[10,11] Ö. Çelik,[18,19,20] E. Charles,[3] A. Chekhtman,[21]‡ C. C. Cheung,[22]‡ J. Chiang,[3] S. Ciprini,[23,11] R. Claus,[3] I. Cognard,[24] J. Cohen-Tanugi,[25] L. R. Cominsky,[26] F. de Palma,[12,13] C. D. Dermer,[27] E. do Couto e Silva,[3] M. Dormody,[28] P. S. Drell,[3] R. Dubois,[3] D. Dumora,[29] C. M. Espinoza,[30] C. Favuzzi,[12,13] S. J. Fegan,[14] E. C. Ferrara,[18] W. B. Focke,[3] P. Fortin,[14] Y. Fukazawa,[31] P. Fusco,[12,13] F. Gargano,[13] D. Gasparrini,[32] N. Gehrels,[18] S. Germani,[10,11] N. Giglietto,[12,13] F. Giordano,[12,13] M. Giroletti,[33] T. Glanzman,[3] G. Godfrey,[3] I. A. Grenier,[4] M.-H. Grondin,[34,35] J. E. Grove,[27] L. Guillemot,[1] S. Guiriec,[36] D. Hadasch,[15] A. K. Harding,[18] G. Jóhannesson,[37] A. S. Johnson,[3] T. J. Johnson,[18,22,45,2]†‡ S. Johnston,[38] H. Katagiri,[39] J. Kataoka,[40] M. Keith,[38] M. Kerr,[3] J. Knödlseder,[41,3] M. Kramer,[30,1] M. Kuss,[9] J. Lande,[3] L. Latronico,[43] S.-H. Lee,[44] M. Lemoine-Goumard,[29] F. Longo,[5,6] F. Loparco,[12,13] M. N. Lovellette,[27] P. Lubrano,[10,11] A. G. Lyne,[30] R. N. Manchester,[38] M. Marelli,[17] M. N. Mazziotta,[13] J. E. McEnery,[18,45] P. F. Michelson,[3] T. Mizuno,[31] A. A. Moiseev,[19,45] C. Monte,[12,13] M. E. Monzani,[3] A. Morselli,[46] I. V. Moskalenko,[3] S. Murgia,[3] T. Nakamori,[40] P. L. Nolan,[3] J. P. Norris,[47] E. Nuss,[25] T. Ohsugi,[48] A. Okumura,[3,49] N. Omodei,[3] E. Orlando,[3,50] M. Ozaki,[49] D. Paneque,[51,3] D. Parent,[2]†‡ M. Pesce-Rollins,[9] M. Pierbattista,[4] F. Piron,[25] T. A. Porter,[3] S. Rainò,[12,13] S. M. Ransom,[52] P. S. Ray,[27] A. Reimer,[53,3] O. Reimer,[53,3] T. Reposeur,[29] S. Ritz,[28] R. W. Romani,[3] M. Roth,[54] H. F.-W. Sadrozinski,[28] P. M. Saz Parkinson,[28] C. Sgrò,[9] R. Shannon,[38] E. J. Siskind,[55] D. A. Smith,[29] P. D. Smith,[56] P. Spinelli,[12,13] B. W. Stappers,[30] D. J. Suson,[57] H. Takahashi,[48] T. Tanaka,[3] T. M. Tauris,[58,1] J. B. Thayer,[3] G. Theureau,[24] D. J. Thompson,[18] S. E. Thorsett,[59] L. Tibaldo,[7,8] D. F. Torres,[15,60] G. Tosti,[10,11] E. Troja,[18] J. Vandenbroucke,[3] A. Van Etten,[3] V. Vasileiou,[25] C. Venter,[61]† G. Vianello,[3,62] N. Vilchez,[41,42] V. Vitale,[46,63] A. P. Waite,[3] P. Wang,[3] K. S. Wood,[27] Z. Yang,[64,65] M. Ziegler,[28] S. Zimmer[64,65]

[1]Max-Planck-Institut für Radioastronomie, Auf dem Hügel 69, 53121 Bonn, Germany. [2]Center for Earth Observing and Space Research, College of Science, George Mason University, Fairfax, VA 22030, USA. [3]W. W. Hansen Experimental Physics Laboratory, Kavli Institute for Particle Astrophysics and Cosmology, Department of Physics and SLAC National Accelerator Laboratory, Stanford University, Stanford, CA 94305, USA. [4]Laboratoire AIM (Astrophysique, Instrumentation et Modélisation), CEA-IRFU/CNRS/Université Paris Diderot, Service d'Astrophysique, CEA Saclay, 91191 Gif sur Yvette, France. [5]Istituto Nazionale di Fisica Nucleare, Sezione di Trieste, I-34127 Trieste, Italy. [6]Dipartimento di Fisica, Università di Trieste, I-34127 Trieste, Italy. [7]Istituto Nazionale di Fisica Nucleare, Sezione di Padova, I-35131 Padova, Italy. [8]Dipartimento di Fisica "G. Galilei," Università di Padova, I-35131 Padova, Italy. [9]Istituto Nazionale di Fisica Nucleare, Sezione di Pisa, I-56127 Pisa, Italy. [10]Istituto Nazionale di Fisica Nucleare, Sezione di Perugia, I-06123 Perugia, Italy. [11]Dipartimento di Fisica, Università degli Studi di Perugia, I-06123 Perugia, Italy. [12]Dipartimento di Fisica "M. Merlin" dell'Università e del Politecnico di Bari, I-70126 Bari, Italy. [13]Istituto Nazionale di Fisica Nucleare, Sezione di Bari, 70126 Bari, Italy. [14]Laboratoire Leprince-Ringuet, École Polytechnique, CNRS/IN2P3, Palaiseau, France. [15]Institut de Ciències de l'Espai (IEEE-CSIC), Campus UAB, 08193 Barcelona, Spain. [16]Columbia Astrophysics Laboratory, Columbia University, New York, NY 10027, USA. [17]INAF-Istituto di Astrofisica Spaziale e Fisica Cosmica, I-20133 Milano, Italy. [18]NASA Goddard Space Flight Center, Greenbelt, MD 20771, USA. [19]Center for Research and Exploration in Space Science and Technology (CRESST) and NASA Goddard Space Flight Center, Greenbelt, MD 20771, USA. [20]Department of Physics and Center for Space Sciences and Technology, University of Maryland Baltimore County, Baltimore, MD 21250, USA. [21]Artep Inc., 2922 Excelsior Springs Court, Ellicott City, MD 21042, USA. [22]National Research Council Research Associate, National Academy of Sciences, Washington, DC 20001, USA. [23]Agenzia Spaziale Italiana (ASI) Science Data Center, I-00044 Frascati (Roma), Italy. [24]Laboratoire de Physique et Chimie de l'Environnement, LPCE UMR 6115 CNRS, F-45071 Orléans Cedex 02, and Station de radioastronomie de Nançay, Observatoire de Paris, CNRS/INSU, F-18330 Nançay, France. [25]Laboratoire Univers et Particules de Montpellier, Université Montpellier 2, CNRS/IN2P3, Montpellier, France. [26]Department of Physics and Astronomy, Sonoma State University, Rohnert Park, CA 94928–3609, USA. [27]Space Science Division, Naval Research Laboratory, Washington, DC 20375–5352, USA. [28]Santa Cruz Institute for Particle Physics, Department of Physics and Department of Astronomy and Astrophysics, University of California at Santa Cruz, Santa Cruz, CA 95064, USA. [29]Université Bordeaux 1, CNRS/IN2p3, Centre d'É tudes Nucléaires de Bordeaux Gradignan, 33175 Gradignan, France. [30]Jodrell Bank Centre for Astrophysics, School of Physics and Astronomy, The University of Manchester, M13 9PL, UK. [31]Department of Physical Sciences, Hiroshima University, Higashi-Hiroshima, Hiroshima 739-8526, Japan. [32]ASI Science Data Center, I-00044 Frascati (Roma), Italy. [33]INAF Istituto di Radioastronomia, 40129 Bologna, Italy. [34]Max-Planck-Institut für Kernphysik, D-69029 Heidelberg, Germany. [35]Landessternwarte, Universität Heidelberg, Königstuhl, D 69117 Heidelberg, Germany. [36]Center for Space Plasma and Aeronomic Research (CSPAR), University of Alabama in Huntsville, Huntsville, AL 35899, USA. [37]Science Institute, University of Iceland, IS-107 Reykjavik, Iceland. [38]Commonwealth Scientific and Industrial Research Organisation, Astronomy and Space Science, Australia Telescope National Facility, Epping NSW 1710, Australia. [39]College of Science, Ibaraki University, 2-1-1, Bunkyo, Mito 310-8512, Japan. [40]Research Institute for Science and Engineering, Waseda University, 3-4-1, Okubo, Shinjuku, Tokyo 169-8555, Japan. [41]CNRS, Research Institute in Astrophysics and Planetology (IRAP), F-31028 Toulouse cedex 4, France. [42]Galaxies, Astrophysique des Hautes Energies et Cosmologie, Université de Toulouse, UPS-OMP, IRAP, Toulouse, France. [43]Istituto Nazionale di Fisica Nucleare, Sezioine di Torino, I-10125 Torino, Italy. [44]Yukawa Institute for Theoretical Physics, Kyoto University, Kitashirakawa Oiwake-cho, Sakyo-ku, Kyoto 606-8502, Japan. [45]Department of Physics and Department of Astronomy, University of Maryland, College Park, MD 20742, USA. [46]Istituto Nazionale di Fisica Nucleare, Sezione di Roma "Tor Vergata," I-00133 Roma, Italy. [47]Department of Physics, Boise State University, Boise, ID 83725, USA. [48]Hiroshima Astrophysical Science Center, Hiroshima University, Higashi-Hiroshima, Hiroshima 739-8526, Japan. [49]Institute of Space and Astronautical Science, JAXA, 3-1-1 Yoshinodai, Chuo-ku, Sagamihara, Kanagawa 252-5210, Japan. [50]Max-Planck-Institut für Extraterrestrische Physik, 85748 Garching, Germany. [51]Max-Planck-Institut für Physik, D-80805 München, Germany. [52]National Radio Astronomy Observatory (NRAO), Charlottesville, VA 22903, USA. [53]Institut für Astro- und Teilchenphysik and Institut für Theoretische Physik, Leopold-Franzens-Universität Innsbruck, A-6020 Innsbruck, Austria. [54]Department of Physics, University of Washington, Seattle, WA 98195–1560, USA. [55]NYCB Real-Time Computing Inc., Lattingtown, NY 11560–1025, USA. [56]Department of Physics, Center for Cosmology and Astro-Particle Physics, The Ohio State University, Columbus, OH 43210, USA. [57]Department of Chemistry and Physics, Purdue University Calumet, Hammond, IN 46323-2094, USA. [58]Argelander-Institut für Astronomie, Universität Bonn, 53121 Bonn, Germany. [59]Department of Physics, Willamette University, Salem, OR 97031, USA. [60]Institució Catalana de Recerca i Estudis Avançats (ICREA), Barcelona, Spain. [61]Centre for Space Research, North-West University, Potchefstroom Campus, Private Bag X6001, 2520 Potchefstroom, South Africa. [62]Consorzio Interuniversitario per la Fisica Spaziale (CIFS), I-10133 Torino, Italy. [63]Dipartimento di Fisica, Università di Roma "Tor Vergata," I-00133 Roma, Italy. [64]Department of Physics, Stockholm University, AlbaNova, SE-106 91 Stockholm, Sweden. [65]The Oskar Klein Centre for Cosmoparticle Physics, AlbaNova, SE-106 91 Stockholm, Sweden.

‡Resident at Naval Research Laboratory, Washington, DC 20375, USA.

Supporting Online Material

www.sciencemag.org/cgi/content/full/science.1207141/DC1
Materials and Methods
Figs. S1 and S2
Tables S1 and S2
References (*33*–*55*)

18 April 2011; accepted 4 October 2011
Published online 3 November 2011;
10.1126/science.1207141

A Homonuclear Molecule with a Permanent Electric Dipole Moment

W. Li,[1,2] T. Pohl,[2] J. M. Rost,[2] Seth T. Rittenhouse,[3] H. R. Sadeghpour,[3]* J. Nipper,[4] B. Butscher,[4] J. B. Balewski,[4] V. Bendkowsky,[4] R. Löw,[4] T. Pfau[4]

Permanent electric dipole moments in molecules require a breaking of parity symmetry. Conventionally, this symmetry breaking relies on the presence of heteronuclear constituents. We report the observation of a permanent electric dipole moment in a homonuclear molecule in which the binding is based on asymmetric electronic excitation between the atoms. These exotic molecules consist of a ground-state rubidium (Rb) atom bound inside a second Rb atom electronically excited to a high-lying Rydberg state. Detailed calculations predict appreciable dipole moments on the order of 1 Debye, in excellent agreement with the observations.

An electric dipole moment forms in classical systems as the result of a separation between opposite charges. A permanent dipole moment of a quantum object requires both the charge separation and degenerate opposite-parity eigenstates. If parity and time reversal

symmetry hold, then an elementary particle cannot have a permanent dipole moment (*1*, *2*). This tenet also holds for more complex objects such as molecules, for which dipole moments can generally arise from differences in the electronegativity of the molecular constituents. Symmetry arguments establish that even polar molecules in their nondegenerate rotational ground state show a weak-field quadratic Stark effect (*3*) due to an induced dipole moment in the laboratory-fixed frame. When an electric field mixes states of opposite parity in a polar molecule, a linear Stark shift occurs, indicating the presence of a permanent dipole moment in the lab-fixed frame. Such dipole moments are crucial in determining the physical and chemical properties of molecular matter. For instance, the dipole moment of ultracold heteronuclear dimers (*4*, *5*), such as KRb, has recently been used to steer chemical reactions (*6*) and opens perspectives for quantum many-body physics, quantum information science, and ultracold chemistry (*7*). These applications are largely based on a sizable dipole moment (*8*), which is commonly precluded in homonuclear molecules. Particle exchange symmetry dictates that a homonuclear molecule cannot have a permanent electric dipole moment, even in the body-fixed frame of reference.

On the other hand, Greene *et al*. (*9*) predicted a decade ago that homonuclear Rydberg molecules can develop a permanent dipole moment due to both the degeneracy of the underlying atomic Rydberg states and a small rotational constant. Rydberg states are highly excited metastable electronic states with large principal quantum number, *n*. Greene *et al*. suggested that a class of diatomic molecule could form at large distances (~1000 Bohr radii) between one atom excited to a Rydberg state and another in the electronic ground state. Such molecules have since been experimentally realized using ultracold rubidium atoms (*10*). However, the *ns* Rydberg state in Rb is well isolated from other electronic levels because of a large quantum defect. These particular molecules were thus expected to have a spherically symmetric, nondegenerate electronic wave function with low angular momentum ($l = 0$) that would preclude the existence of a permanent electric dipole moment (*9*). Initial experimental observations (*9*) were not able to resolve a linear behavior at small electric fields; therefore, the spectra were interpreted by assuming that any manifested Stark shift would be quadratic (arising from an induced dipole moment), similar to the atomic line (fig. S1).

Here, we show that the interaction of the Rydberg electron with the ground-state atom in these Rb diatomics fractionally admixes a nearly degenerate electronic manifold. This admixture localizes the electron density in a region near the ground-state perturber (Fig. 1, A and B), producing a permanent dipole moment in the body-fixed frame of the homonuclear molecule, even in the electronically nondegenerate *ns* state with lowest angular momentum. This permanent electric dipole moment in the body-fixed frame manifests itself in our high-resolution spectroscopic measurements as a linear Stark shift of the molecular lines, allowing us to extract its strength. We augment this surprising observation with detailed theoretical calculations to quantitatively reproduce the experimental findings, and to explain the underlying physics that gives rise to the permanent dipole moment. Symmetry breaking in this homonuclear Rydberg molecule is predicated on the fact that within the total molecular linewidth, measured to be 142 kHz (*11*), rotational and gerade and ungerade splittings remain unresolved, and the linear Stark effect emerges only upon the application of a tiny electric field (*12*). This is equivalent to taking 7-μs snapshots of the molecule during which the dipole moment only rotates through a negligibly small angle with respect to the external field, limited by the lifetime of the molecule (*11*).

The chemical bond in these molecules derives from frequent interactions between the orbiting Rydberg electron and a nearby ground-state perturber, which ultimately binds within

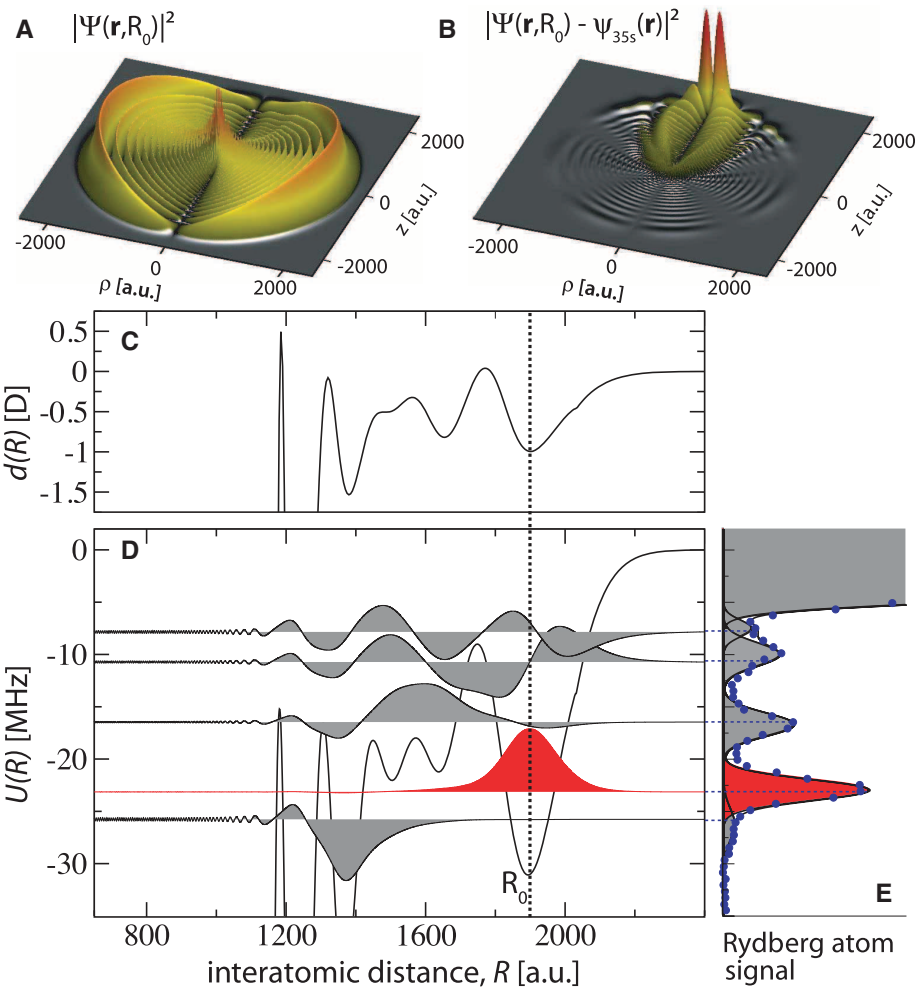

Fig. 1. Calculated electronic Rydberg state, molecular potential curve, and dipole moment of a long-range rubidium $^3\Sigma(5s - 35s)$ molecule. (**A**) The Rydberg electron density at an internuclear distance $z = R_0 \approx 1900$ a.u. ($\rho = 0$ a.u.), marked by the vertical dotted line in (C) and (D). (**B**) Subtracting the bare Rydberg atom wave function reveals a pronounced perturbation that is strongly localized around the perturbing ground-state atom and resembles the structure of the trilobite state of high-*l* Rydberg molecules, scaled by a factor of 200; the ground-state atom is at $z = R_0$ and $\rho = 0$. (**C**) This charge localization results in an appreciable molecular dipole moment, plotted as a function of the internuclear distance. (**D**) The molecular potential and molecular vibrational states bound on the extended potential plateau. (**E**) The molecular excitation spectrum shows good agreement with (D). For the major part of this work, we focus on the vibrational state marked in red, as it has a simple localized vibrational wave function $\chi_0(R)$ (D) and yields the strongest experimental signal (E).

[1]School of Physics and Astronomy, University of Nottingham, Nottingham NG7 2RD, UK. [2]Max-Planck-Institut für Physik komplexer Systeme, Noethnitzer Str. 38, 01187 Dresden, Germany. [3]Institute for Theoretical Atomic, Molecular and Optical Physics (ITAMP), Harvard-Smithsonian Center for Astrophysics, 60 Garden Street, Cambridge, MA 02138, USA. [4]Physikalisches Institut, Universität Stuttgart, Pfaffenwaldring 57, 70569 Stuttgart, Germany.

*To whom correspondence should be addressed. E-mail: hrs@cfa.harvard.edu

the Rydberg atom. Because of the large extent of the Rydberg electron wave function and the electron's low kinetic energy, the interaction that leads to binding can be formally written as a zero-range Fermi pseudopotential interaction (with an energy-dependent scattering length) of a low-energy electron with the ground-state atom (*13*, *14*). In atomic units, this interaction takes the form

$$\hat{V}_{ea}(\mathbf{r},\ \mathbf{R}) = 2\pi A_s(k)\delta(\mathbf{r}-\mathbf{R}) + 6\pi A_p(k)^3\delta(\mathbf{r}-\mathbf{R})\overleftarrow{\nabla}\cdot\overrightarrow{\nabla} \quad (1)$$

for *s*-wave and *p*-wave electron ground-state atom scattering, where $A_s(k)$ and $A_p(k)$ are the respective energy-dependent scattering lengths, and **r** and **R** denote the position of the Rydberg electron and the ground-state atom relative to the Rydberg atom core. Within the semiclassical picture (*14*), the electron momentum k can be related to the intramolecular distance R via energy conservation according to $E_b = (k^2/2) - (1/R)$, where E_b is the binding energy of the isolated Rydberg atom.

To describe our cold rubidium atom experiments, we use the corresponding triplet spin ($S = 1$) electron-atom scattering lengths (*15*, *16*) and diagonalize the molecular Hamiltonian resulting from the interaction operator (Eq. 1) using atomic basis states (*17*). This yields the molecular potentials $U(R)$ (Fig. 1D) and the electronic Rydberg wave functions $\Psi(\mathbf{r}, R)$.

The total electronic spin is restricted to $S = 1$ because the associated *s*-wave scattering length is negative for the electron-rubidium system, whereas the $S = 0$ scattering length is positive and does not lead to molecular binding. The total electronic angular momentum has no component $\Lambda = 0$ along the internuclear axis, because the Rb valence electrons are in states with zero angular momentum, resulting in $^3\Sigma$ molecular symmetry. At large distances, *s*-wave scattering dominates in Eq. 1, and the potentials closely mimic the oscillations of the Rydberg electronic density. Deep potential wells form that can support one stable localized vibrational state in the outermost well near $R \approx 1900$ atomic units (a.u.) (*10*). In *p*-wave electron-alkali atom scattering, there is a broad shape resonance; for e^--Rb(5*s*), this resonance occurs at $k^2/2 = 23.6$ meV (*15*), causing a sharp drop of the molecular potential at $R \approx 1200$ a.u. (Fig. 1D). As a result, there are additional vibrational states delocalized over several hundreds of Bohr radii (*16*) that were resolved earlier (*10*) in field-free measurements (Fig. 1E). The strongest observed molecular line, highlighted in red in Fig. 1, D and E, belongs to the localized wave function $\chi_0(R)$ in the outer well and is the main focus of this work.

The Rydberg electron density of a $^3\Sigma(5s - 35s)$ Rb_2 molecule is shown in Fig. 1A at the equilibrium interatomic separation $R = 1900$ a.u. In Fig. 1B, the corresponding bare Rydberg state 35*s* is subtracted to highlight the asymmetry of the charge distribution. Although the density perturbations are small, they are highly localized at large distances, leading to a sizable permanent electric dipole moment $d(R) = \langle\Psi(R, r)|z|\Psi(R, r)\rangle$ (Fig. 1C).

The total dipole moment of the molecule is found from the expectation value of $d(R)$ over the vibrational wave function, $\chi_0(R)$. The resulting molecular dipoles are shown in Fig. 2A as a function of the effective principal quantum number $n^* = n - \delta_s$, where $\delta_s = 3.13$ is the *s*-wave quantum defect of Rb, revealing a strong decrease with n^*. At first glance, this dependence contrasts with the standard behavior of Rydberg atoms whose response to external fields is known to increase with excitation (*18*). Here, the molecular dipole decreases as $1/n^{*2}$—that is, inversely to the familiar $\sim n^{*2}$ Coulomb scaling of atomic dipole moments.

The scaling of the dipole moments can be established by first assuming that the isotropic *ns* wave function, $\psi_{ns}(\mathbf{r})$, mixes with a nearby degenerate manifold, $\psi_{nT}(R, \mathbf{r})$, according to

$$\Psi(R,\ \mathbf{r}) = \psi_{ns}(\mathbf{r}) + \varepsilon(R)\psi_{nT}(R,\ \mathbf{r}) \quad (2)$$

at an internuclear distance R. The electronic wave function ψ_{nT} (trilobite state) is a linear combination of degenerate states with maximum probability density at the position of the ground Rb(5*s*) atom. The R-dependent permanent dipole moment is then $d(R) = \varepsilon(R)^2 d_T(R)$, where $d_T(R) \sim n^{*2}$ is the permanent dipole moment in the degenerate manifold (*9*). The contribution to the outer-well potential from the *p*-wave scattering phase shift is minimal, so that we need only concern ourselves with the *s*-wave electron scattering contribution in Eq. 1.

Applying first-order perturbation theory to the *s*-wave interaction yields a scaling behavior for the coefficient $\varepsilon(R) \propto A_s\psi_{nT}(R, R)/\mu_s$, where $\mu_s = 0.13$ is the noninteger part of the *s*-wave quantum defect. Because $\psi_{nT}(R, R)$ scales as n^{*-2} (*9*), the scaling for the permanent dipole moment of the homonuclear molecule is $d(R) \sim 1/n^{*2}$, as observed experimentally and in the numerical calculations. For the dipole moment to exist, it is not strictly necessary to couple to a degenerate manifold. For instance, a nondegenerate *p*-state can also couple to the *s*-state to form a permanent dipole moment. However, the size of the dipole moment will be much smaller than that observed and will decrease faster with n^*, as $1/n^{*4}$.

We explored the existence of a permanent dipole moment by measuring the molecular Stark effect in static electric fields. Our molecules are created via photoassociation in a cloud of magnetically trapped ultracold ^{87}Rb atoms, as detailed in (*11*, *16*). The atoms are prepared in their spin-polarized $5S_{1/2}$, $m_F = 2$ ground state at a peak density of $\rho = 10^{13}$ cm^{-3} and a temperature $T = 3$ μK. They are subsequently excited to $nS_{1/2}$ Rydberg states by two-photon excitation via their $5P_{3/2}$ intermediate state with a narrow total laser linewidth $\Delta\nu \leq 100$ kHz. Following their excitation, we detect the Rydberg atoms by electric field ionization and record the excitation spectrum by varying the two-photon detuning of our excitation lasers.

In the present experiments, we observed a series of resonances to the red (lower-frequency side) of the atomic transition that matched our theoretical predictions and could thus be attributed

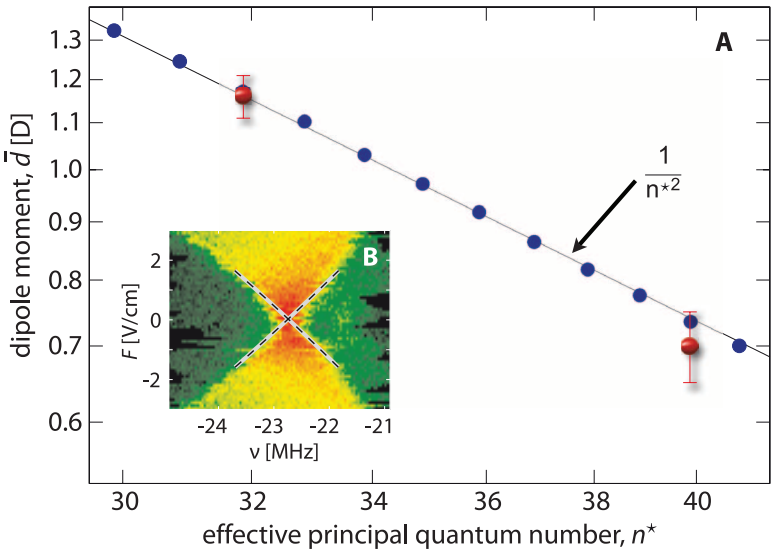

Fig. 2. (**A**) The molecular permanent electric dipole moments $\bar{d} = \langle\chi_0(R)|d(R)|\chi_0(R)\rangle$ of the outermost localized vibration state in rubidium $^3\Sigma(5s - ns)$ as a function of the effective principal quantum number n^*. The blue dots show the result of the numerical calculations; the red dots represent the experimental values obtained from fits to our measured Stark spectra, as shown in (B) for $n = 35$. The error bars denote the standard deviation of the fit parameter for the dipole moment. As opposed to the familiar $\sim n^{*2}$ Rydberg scaling of atomic dipole moments, the strength of the molecular dipole moment decreases as $\sim 1/n^{*2}$. The line is a $1/n^{*2}$ fit to the results. (**B**) The observed two-dimensional Stark spectrum of the corresponding molecular state for $n = 35$ at small electric fields. The dashed lines are the fitted linear Stark shifts (see text).

to direct photoassociation of the long-range molecular states. To probe their Stark shift, we applied electric fields (up to 9 V/cm) that were well below the field ionization threshold of the excited Rydberg states during the excitation. All of the observed resonances showed a strong quadratic Stark shift that originates from the large polarizability of the bare, unperturbed Rydberg atoms (*16*). To extract the molecular contribution, we used the measured shift of the atomic excitation line to subtract the bare atom shift from the data (*17*).

A high-resolution spectrum for small electric fields up to 3 V/cm is shown in Fig. 2B. Instead of isolated, Stark-split rotational lines, we observed a continuous Stark fan whose broadening is linear down to the smallest applied fields. To determine the permanent dipole moment, we found for each electric field the points at which the Rydberg signal had dropped to half its maximal value. A fit to a second-order polynomial (dashed lines in Fig. 2B) yields the permanent electric dipole moment as the gradient at zero electric field and gives 1.16 (±0.05) D for the $^3\Sigma(5s - 35s)$ molecule and 0.70 (±0.05) D for the $^3\Sigma(5s - 43s)$ state. The theoretical values of 1.17D and 0.75D are in excellent agreement with the observed dipole moment (Fig. 2A).

Stark maps for additional states were also observed as weak resonances (Fig. 3C). For direct theoretical comparison, we also calculated the Stark spectra of higher vibrational molecular states by adapting the inward scattering approach in (*16*) to multichannel scattering in order to account for the electric-field coupling among the different rotational states (*17*). Figure 3A shows the resulting spectrum of ro-vibrational states, convolved with the atomic natural line profile measured in (*19*). This bare spectrum shows additional states not observed in the experiment, as it does not account for the finite linewidth of the Rydberg excitation and the small Franck-Condon overlap of the initial and final states. Upon incorporating these factors, the resulting photoassociation spectrum calculated at $T = 3$ μK, shown in Fig. 3B, is in remarkable agreement with our measurements (Fig. 3C) without any adjustable parameters.

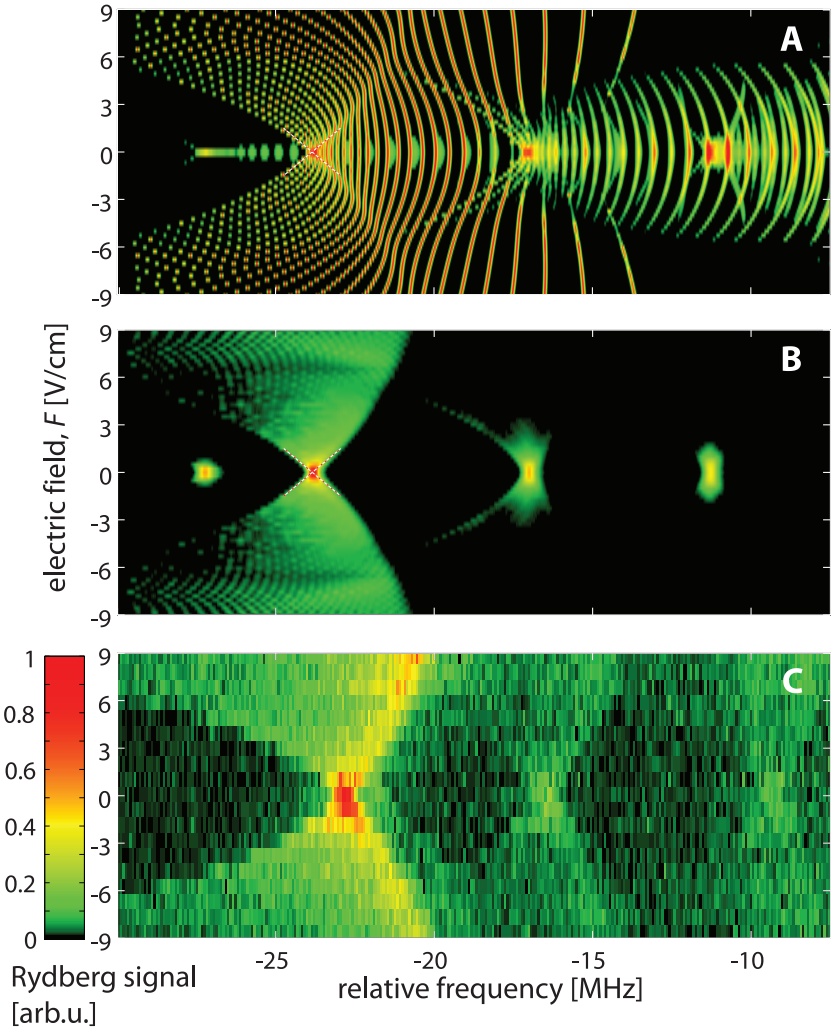

Fig. 3. Two-dimensional Stark spectra of $^3\Sigma(5s - 35s)$ rubidium molecules. The zero of the frequency axis is the atomic Rydberg state. (**A**) The ro-vibrational lines for several angular states calculated according to their theoretically predicted minimum linewidth. (**B**) The theoretical photoassociation using the transition linewidth determined in (*16*), upon thermal averaging. Note that many of the states shown in (A) are not present because of the vanishing angular overlap with the initial thermal gas state. (**C**) Our measured Stark spectrum is in good quantitative agreement with the predicted spectrum.

In view of the symmetry arguments outlined above, the excellent agreement between experiment and theory might seem surprising at first. However, the calculation of the permanent dipole moment (Fig. 2) assumes that there is no exchange symmetry in the body-fixed frame of the molecule, and the experimental observation of a linear Stark shift confirms this assumption. In contrast, for a molecule consisting of identical atoms, both parity and exchange symmetries clearly prohibit the existence of a permanent dipole moment in both the body-fixed and laboratory frames. The resolution to this dilemma lies in the vast length scale disparity between the ground-state and Rydberg-state atoms. Unlike in more generic homonuclear molecules, for which the density of each electron is spread over the entire extent of the molecule, the ground-state atom in the present case is orders of magnitude smaller then the molecule itself. As a consequence, the parity eigenstates of $^3\Sigma_g$ and $^3\Sigma_u$ symmetry are nearly degenerate, as the corresponding exchange splitting Δ_{xc} is proportional to the tunneling amplitude of the ground-state electron between the far distant atomic cores. For the Rb_2 Rydberg molecules, this implies a tremendous delocalization time scale longer than the age of the universe, such that parity symmetry is broken under the influence of any measurable external field. The molecules are therefore produced directly in charge-localized states that carry a body-fixed dipole moment.

Although the value of this dipole moment, $\bar{d} \approx 1$D (for $n = 35$), is comparable to that of the heteronuclear ground-state dimers, the corresponding rotational constant $B \approx 11.5$ kHz is several orders of magnitude smaller than that for a typical molecule such as KRb ($B \approx 1$ GHz) (*4*). Hence, the effect here of electric fields of up to 9 V/cm is equivalent to fields of ~1 MV/cm applied to more conventional, ground-state, polar molecules, which is known to result in highly localized, field-aligned pendular states (*20*–*23*). However, the rotational constant of the Rydberg molecule is considerably smaller than the excitation linewidth of the molecular state [142 kHz (*11*)]. This results in direct excitation of localized rotational wave packets (*24*, *25*) of varying orientation, which remain static on the time scale of the experiment, producing a broad Stark fan with a linear spread of $\pm \bar{d}F$, as observed at small electric fields.

The existence of a permanent dipole moment in long-range Rydberg molecules opens up possibilities for experimental control. For instance, the resulting sensitivity to external electric fields may provide a valuable tool for experimental

analysis of the structure of more complex polyatomic compounds (*26*–*29*). Whereas the discussed scaling behavior is generic to all alkali metal atoms, the derived $\overline{d} \approx A_s^2/n^{*2}\mu_s^2$ scaling suggests considerable variations of the dipole moments among different atomic species. In particular, cesium, with a smaller noninteger part of the *s*-wave quantum defect (*30*) and a larger *s*-wave scattering length (*31*), might possess a dipole moment of ~15D (larger by an order of magnitude) for the same electronic state discussed above. By the same mechanism described here, we can expect that the molecular electronic states of the so-called trilobite molecules (*9*) admix a small amount of *s*-wave character, possibly making such molecules accessible to a standard two-photon association process. These trilobite molecules are predicted to have much larger permanent dipole moments (on the order of 1 kD), presenting extreme sensitivity to external fields.

References and Notes

1. W. Bernreuther, M. Suzuki, *Rev. Mod. Phys.* **63**, 313 (1991).
2. D. J. Gross, *Proc. Natl. Acad. Sci. U.S.A.* **93**, 14256 (1996).
3. W. Klemperer, K. K. Lehmann, J. K. G. Watson, S. C. Wofsy, *J. Phys. Chem.* **97**, 2413 (1993).
4. K.-K. Ni *et al.*, *Science* **322**, 231 (2008).
5. J. Deiglmayr *et al.*, *Phys. Rev. Lett.* **101**, 133004 (2008).
6. S. Ospelkaus *et al.*, *Science* **327**, 853 (2010).
7. L. Carr, D. DeMille, R. V. Krems, J. Ye, *N. J. Phys.* **11**, 055049 (2009).
8. T. Lahaye, C. Menotti, L. Santos, M. Lewenstein, T. Pfau, *Rep. Prog. Phys.* **72**, 126401 (2009).
9. C. H. Greene, A. S. Dickinson, H. R. Sadeghpour, *Phys. Rev. Lett.* **85**, 2458 (2000).
10. V. Bendkowsky *et al.*, *Nature* **458**, 1005 (2009).
11. B. Butscher *et al.*, *Nat. Phys.* **6**, 970 (2010).
12. M. S. Schöffler *et al.*, *Science* **320**, 920 (2008).
13. E. Fermi, *Nuovo Cim.* **11**, 157 (1934).
14. A. Omont, *J. Phys. (Paris)* **38**, 1343 (1977).
15. E. L. Hamilton, C. H. Greene, H. R. Sadeghpour, *J. Phys. B* **35**, L199 (2002).
16. V. Bendkowsky *et al.*, *Phys. Rev. Lett.* **105**, 163201 (2010).
17. See supporting material on *Science* Online.
18. T. F. Gallagher, *Rydberg Atoms* (Cambridge Univ. Press, Cambridge, 1994).
19. B. Butscher *et al.*, *J. Phys. B* **44**, 184004 (2011).
20. B. Friedrich, D. R. Herschbach, *Nature* **353**, 412 (1991).
21. P. A. Block, E. J. Bohac, R. E. Miller, *Phys. Rev. Lett.* **68**, 1303 (1992).
22. J. M. Rost, J. C. Griffin, B. Friedrich, D. R. Herschbach, *Phys. Rev. Lett.* **68**, 1299 (1992).
23. R. González-Férez, M. Mayle, P. Sánchez-Moreno, P. Schmelcher, *Europhys. Lett.* **83**, 43001 (2008).
24. H. Stapelfeldt, T. Seideman, *Rev. Mod. Phys.* **75**, 543 (2003).
25. T. Seideman, E. Hamilton, *Adv. At. Mol. Opt. Phys.* **52**, 289 (2005).
26. I. C. H. Liu, J. Stanojevic, J. M. Rost, *Phys. Rev. Lett.* **102**, 173001 (2009).
27. S. T. Rittenhouse, H. R. Sadeghpour, *Phys. Rev. Lett.* **104**, 243002 (2010).
28. S. T. Rittenhouse *et al.*, *J. Phys. B* **44**, 184005 (2011).
29. I. C. H. Liu, J. M. Rost, *Eur. Phys. J. D* **40**, 65 (2006).
30. C. J. Lorenzen, K. Niemax, *Z. Phys. A* **315**, 127 (1984).
31. C. Bahrim, U. Thumm, I. I. Fabrikant, *J. Phys. B* **34**, L195 (2001).

Acknowledgments: We thank J. Feist and P. Julienne for useful discussions in the preparation of this work and L. Kukota for her assistance. Supported by NSF grant 0653021 through ITAMP, the Harvard Department of Physics, and the Smithsonian Astrophysical Observatory (S.T.R. and H.R.S.), a European Union Marie Curie Fellowship (W.L.), and the Deutsche Forschungsgemeinschaft within SFB/TRR21 and the project PF 381/4-2.

Supporting Online Material

www.sciencemag.org/cgi/content/full/334/6059/1110/DC1
SOM Text
Fig. S1
References (*32*–*34*)

15 July 2011; accepted 19 October 2011
10.1126/science.1211255

Discovery of an α-Amino C–H Arylation Reaction Using the Strategy of Accelerated Serendipity

Andrew McNally, Christopher K. Prier, David W. C. MacMillan*

Serendipity has long been a welcome yet elusive phenomenon in the advancement of chemistry. We sought to exploit serendipity as a means of rapidly identifying unanticipated chemical transformations. By using a high-throughput, automated workflow and evaluating a large number of random reactions, we have discovered a photoredox-catalyzed C–H arylation reaction for the construction of benzylic amines, an important structural motif within pharmaceutical compounds that is not readily accessed via simple substrates. The mechanism directly couples tertiary amines with cyanoaromatics by using mild and operationally trivial conditions.

Accidental or serendipitous discoveries have led to important breakthroughs in the chemical sciences. With regard to bond-forming reactions, such fundamental synthetic transformations as Friedel-Crafts, Wittig olefination, and Brown hydroboration reactions were found when the objectives of the initial experiments were not in accord with the observed outcomes (*1*).

Recently, we questioned whether serendipity could be forced or simulated to occur on a predictable basis in the realm of reaction discovery, thereby providing a reliable platform to access valuable transformations or unexpected pathways. Herein, we describe the successful execution of these ideals and describe a fundamentally distinct C–H functionalization-arylation reaction that we expect will be of broad use to practitioners of chemical synthesis and, in particular, medicinal chemistry.

Assuming that serendipity is governed by probability (and thereafter manageable by statistics), performing a large number of random chemical reactions must increase the chances of realizing a serendipitous outcome. However, the volume of reactions required to achieve serendipity in a repetitive fashion is likely unsuitable for traditional laboratory protocols that use singular experiments. Indeed, several combinatorial strategies have previously been used to identify singular

Merck Center for Catalysis, Department of Chemistry, Princeton University, Princeton, NJ 08544, USA.

*To whom correspondence should be addressed. E-mail: dmacmill@princeton.edu

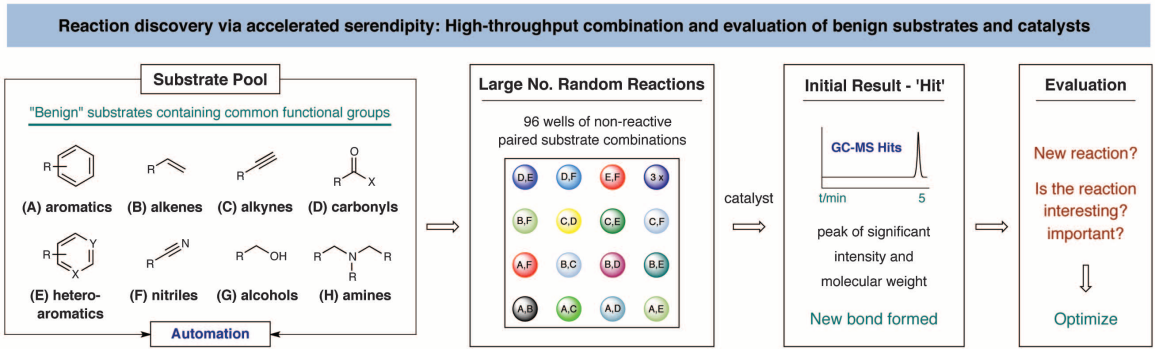

Fig. 1. Approach to reaction discovery without preconceived design via the concept of accelerated serendipity. R indicates a generic organic substituent; X and Y, heteroatoms.